Study on lime dissolution in converter slag

Tengfei Deng and Du Sichen

Department of Materials Science and Engineering, Royal Institute of Technology,

SE-10044 Stockholm, Sweden

Abstract: In order to obtain reliable information of lime dissolution under forced convection, the commonly used rotating rod method was examined. Both CFD calculation and cold model experiments showed evidently that the mass transfer due to radial velocity introduced by forced convection was zero if the rod was centrally placed in a cylindrical container. This finding was in accordance with the criteria put forward by the original work that the method could only be applicable when a thin disk (instead of rod) with big diameter and big liquid bath were used. A new experimental design was therefore developed. A cube was placed in the crucible and stirred by Mo rod along with slag. The whole system, lime and slag, could be quenched in order to maintain the state of the system at high temperature. A linear relationship between normalized length and time was obtained for lime dissolution. Different lime samples showed big difference in dissolution rate. It was found that the main mechanism of CaO dissolution in slag was due to the removal of $2CaO{\cdot}SiO_2$ layer. This removal process was evidentially seen in the vicinity of the lime cube in the quenched slag phase.

Key words: lime, dissolution, slag, stirring

1. Introduction

In BOF process, slag plays a very important role in decarburization and oxidizing reactions. Converter slag contains mostly CaO, SiO_2, MnO, MgO and `FeO´. While $SiO_2$, MnO and `FeO´ come into the slag by oxidation, and CaO in the slag is due to the addition of lime. The content of CaO in the converter slag is quite high, usually between 40 mass% and 50 mass%. Very often, undissolved lime particles are fond in the slag even at the final stage of the converter process. While, the demands on high quality steel and optimization of converter process have greatly emphasized the importance of lime dissolution in converter slag. Fast lime dissolution in slag would ensure the power of the slag for dephosphorisation, shorten the process and reduce the consumption of the raw material as well as energy.

The dissolution of lime and dolomite into different slag systems has been the topic of many researchers [1]-[9]. Russell [1] studied lime reactivity as well as dissolution rates and reported that the dissolution of lime could be determined at room temperature by ASTM water reactivity test. On the other hand, Schlitt and Healy [2] studied the kinetics of lime dissolution in CaO-FeO-SiO_2 slag and found that the rate of lime dissolution was not significantly affected by the density of lime. Hachtel et al. [3] investigated the dissolution of lime single-crystals in FeO-SiO_2 slag and found $2CaO{\cdot}SiO_2$ and $3CaO{\cdot}SiO_2$ phases between slag and CaO surface. Those studies were based on the static state.

The method of rotating cylinder or disk in the slag has been widely used by many researchers [10-24] to study dissolution and erosion. Matsushima et al. [10] studied the dissolution rate of solid lime into liquid slag by rotation rod concentrically placed in crucible. The authors introduced a J-factor to express the mass transfer in liquid. Natalie and

Evans [11] used rotating lime disk in slag to study the relation between the properties of lime and dissolution rate. Singh and Ghosh [12] studied the relation between water reactivity test and lime dissolution in steelmaking slag with half of the length of lime submerged in slag. Unfortunately, all the studies seemed to have neglected the constraints of the method emphasized by Gregory and Riddiford. [25] It must be mentioned that Gregory and Riddiford [25] clearly pointed out that the theory was only applicable to a disk that had very large ratio between diameter and thickness. They also emphasized that the vessel should have theoretically infinite volume.

2. Evaluation of the rotating rod method in high temperature experiment

The essential criteria of using rotating disk method are the big diameter/thickness ratio and the infinite big vessel. [25] These criteria have practically ruled out the use of this technique in the study of lime in slag. It is impossible to have a reaction chamber that can hold crucible with big enough diameter. Therefore, only the rotation rod method is discussed in the present work. For this purpose, both CFD calculation and experiments at room temperature are carried out.

2.1 CFD calculation

In the present study the software package COMSOL Multiphysics 4.2 is used. Considering the possible dimensions of the experimental setup at high temperature, a container with an inner diameter of 44 mm is studied. The height of the liquid in the container is 95 mm. A rod having 8 mm diameter is considered.

A 3D steady state model is employed. The flow is considered turbulent in nature. The equation of continuity, momentum equations and the k-ε model are solved simultaneously with moving mesh. The non-slip condition is employed at the solid walls. A wall function is utilized to simulate the logarithmic velocity profile near the wall. At the upper surface it is assumed that there is no mass transfer to the gas and the shear stresses is zero. Between the liquid domain and rotating domain the flow field is continuous across the pair. The mesh is chosen as a compromise between solver memory requirement and convergence. Consequently the mesh changes slightly within the calculations.

Figure 1 presents the calculated stream lines along with velocity distributions in 4 horizontal sections in the system where the rod is immersed to the bottom of the vessel. The dimensions of the vessel and the length of the immersed rod are schematically given in Figure 1. The vertical positions of the 4 horizontal sections are also marked in this figure. In the calculation, a rotation speed of 100 RPM is used. It is clearly seen in the figures that no radial flow is created by the rotation in any of the sections. One can evidently conclude that mass transfer from the rod to the melt is not enhanced by rotation, if the rod is immersed to the bottom of the liquid. The CFD calculation also shows that in the case of half-way immersed rod, the radial velocity is almost zero above the end of the rod. Below the level of the immersed rod, the radial velocities are also very small (lower than 1.4 $x10^{-3}$ m/s). The increase of the rotation speed would increase the radial velocity below the rod slightly. On the other hand, since there is no radial velocity along the rod, the mass transfer can only be slightly affected by the rotation speed. CFD calculation is also conducted to examine how the non-concentrically placement of the rotating rod affects the mass transfer, as the difficulties of high temperature experiment very often lead to non-concentric placement. The results show that radial flow is created by the non-concentric rotating

rod. The radial velocity can be at the same level of the peripheral component. However, the exact position of the rod must be kept in all the experiments and known in order to analyze the results.

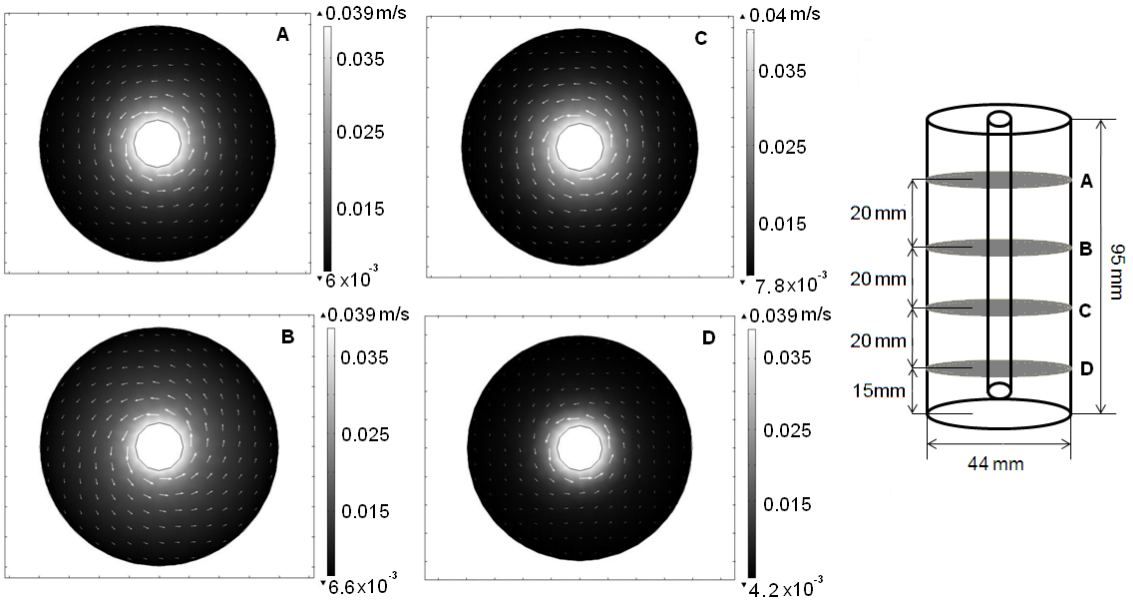

Figure 1 Calculated stream lines along with velocity distributions in 4 horizontal sections at 100 rpm rotation speed in the system where the rod is immersed to the bottom of the vessel

2.2 Verification of the CFD calculation by cold model experiments

To verify the CFD calculation, room temperature experiments were carried out. The dissolution of candy bar in water was used for this purpose. Figure 2 shows schematically the cold model setup. A thermostat kept the cylindrical container made of plastic along with water at 298 K. The container had an inner diameter of 44mm and liquid height of 95mm. A candy bar having an average diameter of 8mm was rotated by a Euro Star motor, which was mounted above the water container. Before the experiment, the diameter of a straight candy bar was measured at a few positions along its length. An average diameter was calculated over all the values. The rod was mounted on the motor. Special care was taken to ensure that the candy rod is mounted vertically. The rod was carefully placed at a predetermined horizontal position. A scale beside the container would measure the immersed length of the rod. The rod was rotated with a constant speed just after the immersion of the rod. The rotation was stopped after a predetermined period. The rod was taken out immediately and its diameter measured at different positions. Note that fresh water and a new candy rod were used in each experiment.

To describe the dissolution, the normalized diameter, D_N defined by eq. [1] is used.

$$D_N = \frac{D}{D_o} \qquad [1]$$

Where, D and D_o stand for the diameter and the initial diameter of the rod. Figure 3 presents the normalized diameter as a function of dissolution time for different rotating speeds. In this series of experiments, the rod was placed at the center of the vessel and the immersed length was 80mm. The experimental points obtained at 0 RPM reveal that dissolution

taking place by only natural convection and diffusion. The figure evidently shows that the contribution to mass transfer by forced convention is almost zero. The result is in excellent agreement with the velocity distributions shown in Figure1, where no radial velocity exists.

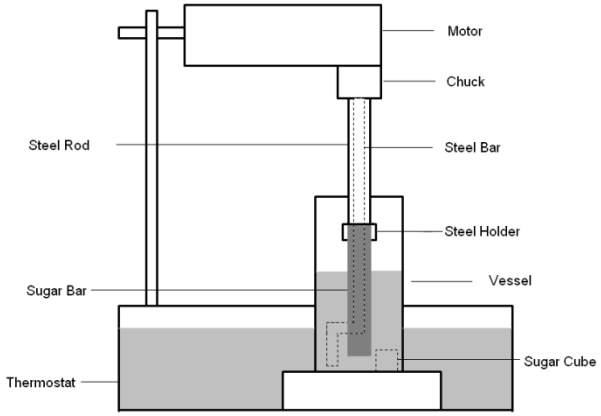

Figure 2 Cold model experiment setup

The results of the experiments with a rod 45 mm concentrically immersed in water shows that the dissolution depends very little on the rotating speed and natural convention is still the dominating mechanism. The radial velocities below the level of the rod are not zero. The radial flow would help the mass transfer to some extents. However, the effect of rotating rate on the dissolution is not profound, since the contribution from natural convention still plays the dominating role. The results of non-concentrically placed rod shows that natural convection still plays the dominating role, though the rotating speed has somewhat effect on the mass transfer. The small effect of rotating rate on dissolution is in line with the velocity distributions predicted by CFD calculation. The radial flow generated by the eccentric placement of the rod enhances the mass transfer. Since the radial velocity is still low at different depths of the liquid, the contribution of forced convection to the mass transfer is limited.

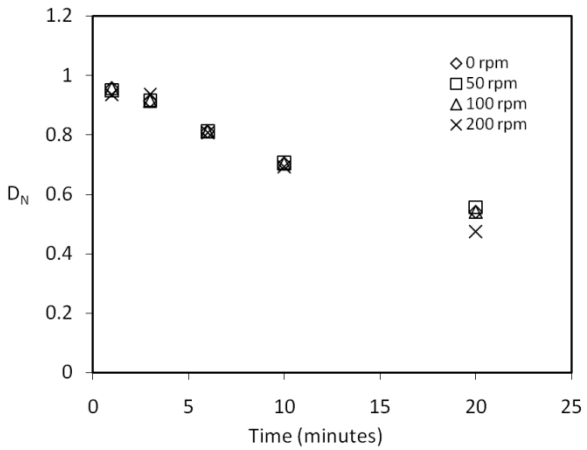

Figure 3 Normalized diameters as a function of dissolution time for different rotating speeds of a whole rod concentrically immersed in water

3. Development of a technique to study lime dissolution

Whether dissolution of lime in slag with convection continues by the dissolution of this layer into the slag or by mechanical flushing off is still not clear. The real mechanism can be revealed only if the CaO sample along with the slag is quenched from the experimental temperature. Hence, freezing the CaO sample and slag is one of the goals of the new method.

Forced convection is much more dominating than natural convection and diffusion in converter process. As discussed in the last section, the rotating rod technique cannot enhance the mass transfer by forced convection. A new experimental technique should introduce efficient mass transfer by forced convection.

The development of the new technique is carried out in 3 steps, namely CFD calculation, room temperature experiments and high temperature experiments.

3.1 CFD calculation

The preliminary idea of the stirring system is that the liquid bath is stirred by a bar moving circularly in it. The solid phase shaped as cube moves randomly in the liquid bath due to the movement of the liquid. In fact, this kind movement is somehow similar as the movement of lime particles in the slag phase.

To get basic information of the movement of the liquid, CFD simulation is made. Again, the flow is assumed to be steady state and 3 dimensional. The cylindrical container has an inner diameter of 44 mm. The height of the liquid bath is 20 mm. The circularly moving bar that is 15 mm immersed in the liquid moves at a radius of 8 mm.

Figure 4 presents the velocity distributions in the horizontal section in the half height of the bath for rotating speeds 100 rpm. Note that in the new experimental design, the cube of the sample is not situated in the center. As seen in the figures, velocity component perpendicular to the cube always exists. The trajectory of the rod is a circle of 16 mm in diameter. The highest speed is found at the bar. A cube would experience higher velocity when its position is close to the stirring bar. The increase of the stirring speed evidently increases the liquid velocity perpendicular to the cube. This increase is essential in the examination whether mass transfer in the liquid is the controlling step in the dissolution process. In fact, the rotating rod method would not be able to draw this conclusion when the setup is precisely made (exactly concentrically placed).

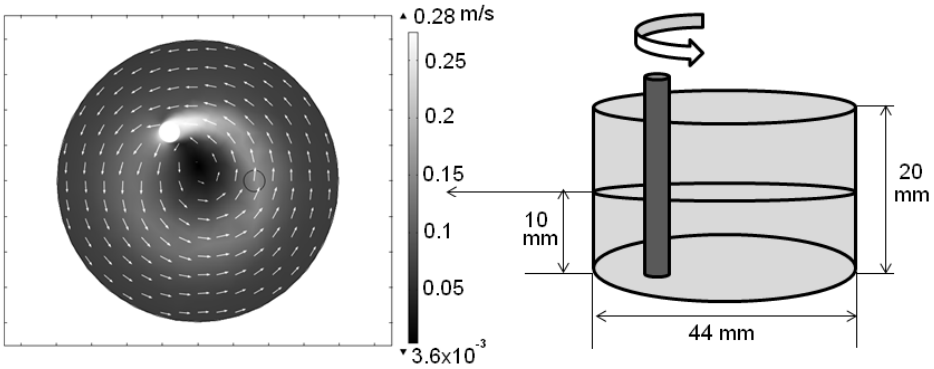

Figure 4 Velocity distributions in the horizontal section in the half height of the bath for 100 rpm rotating speeds

3.2 Room temperature experiments

The experimental setup was similar as the one using rotating rod. However, the bath was stirred by a steel bar moving circularly as shown in Figure 2 with dotted lines. A cube (10×10×10mm) of the same kind of sugar as the rod was moving randomly in the bath. The stirring was stopped after a predetermined period. The cube was taken out immediately and its dimensions were measured. Fresh water and new candy cubes were used in each experiment.

It is worthwhile to mention that the stirring bar was observed only occasionally pushing the sugar cube. This pushing phenomenon usually took place for a few seconds before the cube became apart from the bar again. Since the cube would follow the flow of the liquid, the pushing was relatively gentle and would not mechanically damage the cube.

Figure 5 presents normalized length of the cube L_N as a function of stirring time for different stirring speeds. The normalized length is defined as

$$L_N = \frac{L_1 + L_2 + L_3}{\left[L_1 + L_2 + L_3\right]_o} \qquad [2]$$

Where L_1, L_2 and L_3 are the lengths of three dimensions of the cube, the subscribe 0 denotes the initial stage. In contrast to the rotating rod experiments, the stirring speed does have effect on the dissolution. The higher the stirring speed is, the higher dissolution rate is observed.

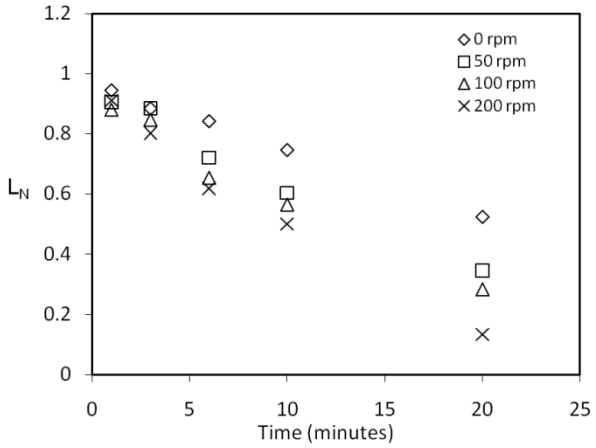

Figure 5 Normalized length of the cube L_N as a function of stirring time for different stirring speeds.

It is difficult to compare the results of the cube and rod quantitatively, since the natural convections of these two cases are very different. On the other hand, a qualitative comparison of the results of the two techniques still reveals that the new method is able to introduce faced convection efficiently, while the rotating rod method is not able to.

3.3 High temperature experiments

As discussed earlier, the new experimental method is not only able to introduce the forced convection, but also able to freeze the whole system, viz. sample and slag. Figure 6 shows schematically the experimental setup. A high temperature vertical furnace with Super-Kanthal heating elements was employed. An alumina tube was used as the reaction chamber with a quenching chamber cooled by water on its top. Argon gas was introduced through the gas inlet

connected to the quenching chamber and led out at the lower end of the chamber. A Euro Star motor was used to drive the stirrer made of molybdenum. In all the experiments, Mo crucible was used to hold the slag and the CaO sample. The Mo crucible was placed in a Mo holder that was hung on a plate. The plate was mounted on a lift which could move both downwards and upwards for introducing the sample and quenching it after reaction. Another small lifting unit with high precision was used to move the stirrer. The second lifting unit was fixed on the main lifting system. The main feature of the setup can be summarized below:

(1) The whole system was gas tight by using O-rings.

(2) The crucible holder along with the crucible could be moved both down and up rapidly by the main lifting system.

(3) The stirrer could be inserted into the melt and removed from it by the second lifting system.

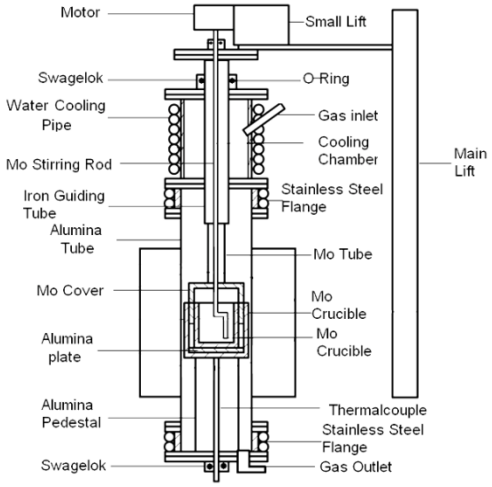

Figure 6 Experimental setup

3.3.1 High temperature experimental procedure

Three types of CaO samples were all prepared by Lhoist using lime stone. The CaO sample was in the form of cube, about 9x9x9 mm in size. The pre-melted slag (30mass%CaO-44mass%FeO-26mass%SiO_2) was crushed into small pieces, a few mm in size. The dimensions of the cube were carefully measured before the cube being embedded in the slag pieces. The slag weighed 15g. The crucible holder with the sample was placed in the low temperature zone of the reaction tube. The reaction chamber was then sealed and flushed with argon gas for at least 60 min. Thereafter, argon flow of about 0.1 L/min was maintained throughout the whole experiment. The sample was heated up to a predetermined temperature, e.g. 1873 K and stabilized. The sample holder was lowered down to the high temperature zone. The pre-melted slag would need 10 sec. to re-melt. [26] After this melting time, the stirring was started. After a given time of stirring, the stirrer was lifted by the precision lift, which took about 1-2 seconds. The slag along with the reacted CaO cube was quenched by lifting the holder to the cooling chamber using the main lifting system.

The Mo crucible along with the sample was then taken out and cut at a vertical position going through the remaining CaO cube. The crucible along with the slag and remaining CaO part was polished. The position of the polished surface was 3 mm from the bottom of the crucible. The section was then subjected to light microscopic (LOM) and scanning microscopic (SEM) analysis.

4. Results of high temperature experiment

Figure 7 presents the normalized length as a function of stirring time at 50 rpm stirring speed at 1873 K. The normalized length, L_N is defined as: [26]

$$L_N = \frac{L_1 + L_2}{(L_1 + L_2)_{initial}} \quad [3]$$

Where $L_1 + L_2$ is the sum of the lengths of the unreacted core in two perpendicular directions of the cross section, while, the subscript "initial" stands for the initial value before the experiment. A linear relationship between normalized length and time is seen in Figure 7. It implies that, the dissolution rate is constant for each type of sample and is independent of CaO concentration in the slag.

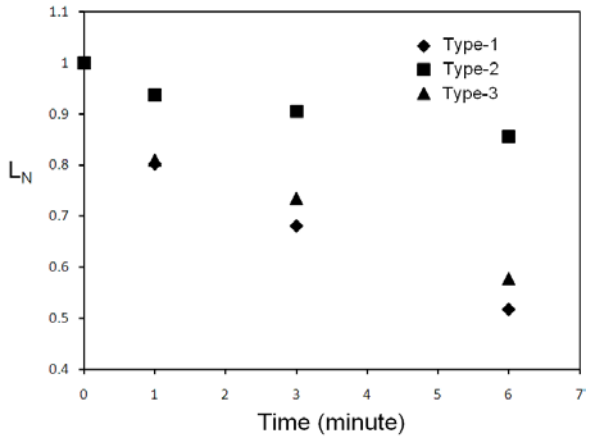

Figure 7 Normalized lengths as a function of stirring time at 50 rpm stirring speed at 1873 K

Figures 8a and 8b present the SEM microphotographs of the interface region between lime cube and slag for Type-1 and Type-2 samples, respectively. Both samples have been kept in the slag at 1873 K and stirred at 50 rpm stirring speed for 3 min. Four main phases are identified in the specimen of Type-1 sample. In addition to the remaining CaO and slag, $2CaO{\cdot}SiO_2$ and $3CaO{\cdot}SiO_2$ have been formed. Slag has penetrated into the CaO matrix close to the interface. However, the penetrating liquid phase has very different composition from the original slag, which is still found beyond the interface region. The liquid phase in the CaO matrix consists of mostly CaO and FeO. Coexistence of $3CaO{\cdot}SiO_2$ with the liquid phase in the CaO matrix is also observed. An explanation of this aspect can be found in the previous publication [26]. There is still a region between slag and CaO, in which liquid, $2CaO{\cdot}SiO_2$ and $3CaO{\cdot}SiO_2$ coexist. This region is about 50-100 μm thick in general.

Similar as the Type-1 sample, the same four phases are also found in Type-2 specimen (see Figure 8b). On the other hand, the amount of liquid phase penetrating into the CaO matrix is very little, much less than that found in the matrix of Type-1 sample that originally has high porosity. Note that even in the case of Type-2 sample, the liquid found in the CaO matrix has mostly CaO and FeO. Even for the dense CaO (Type-2), the interface region consisting of liquid, $2CaO{\cdot}SiO_2$ and $3CaO{\cdot}SiO_2$ can be identified. The thickness of this interface region is about 50-100 μm.

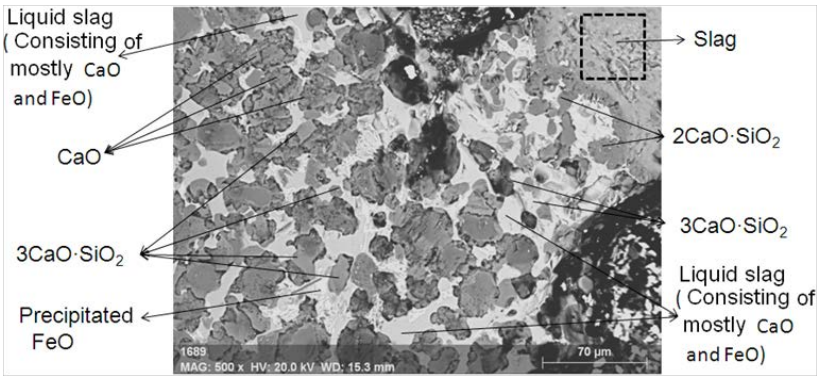

(a)

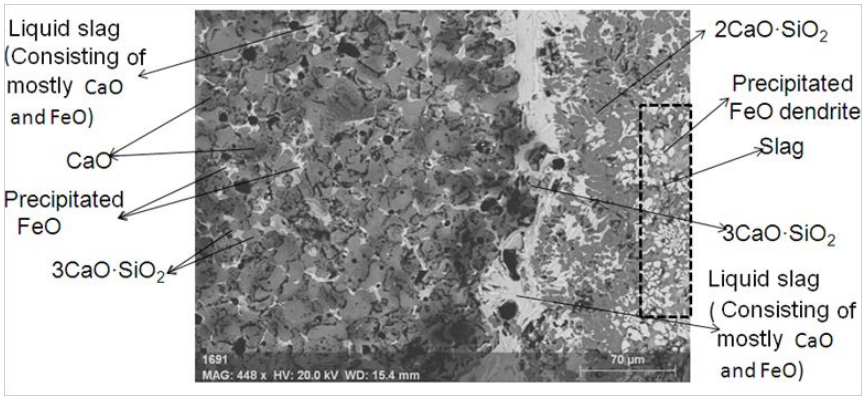

(b)

Figure 8 Interface region between lime cube and slag after experiment at 50 rpm stirring speed for 3 minutes at 1873K (a) type-1 CaO cube, (b) type-2 CaO cube

To understand the effect of stirring speed on the CaO dissolution, the interfaces of Type-1 and Type-2 samples studied at 150 rpm are also examined in SEM. Figures 9a and 9b present the SEM microphotographs of Type-1 and Type-2 samples, respectively. Similar as in the case of 50rpm stirring (see Figures 8a and 8b), the same phases are identified in both of specimens. While the thickness of the interface region of Type-2 sample are comparable at these two stirring speeds (Figure 8b and Figure 9b), the thickness of the region in Type-1 sample is almost negligible at this stirring speed (Figure 9a). This finding is very different from the same CaO (Type-1) stirred at 50 rpm.

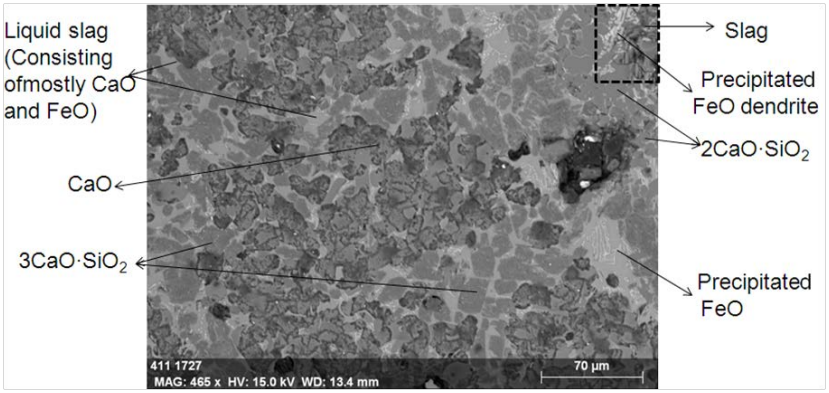

(a)

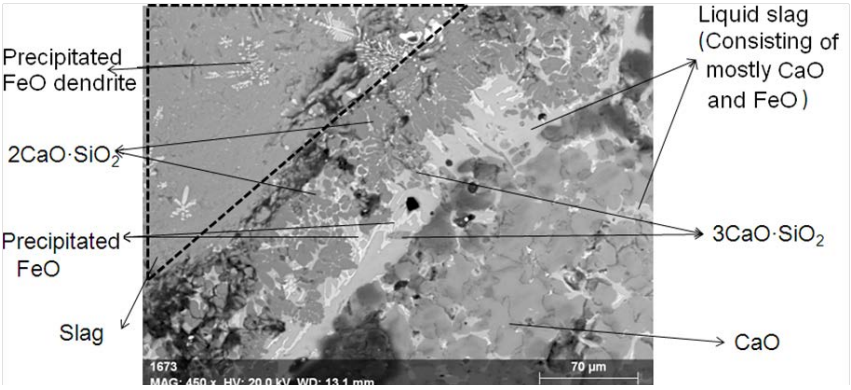

(b)

Figure 9 Interface region between lime cube and slag after experiment at 150 rpm stirring speed for 3 minutes at 1873K (a) type-1 CaO cube, (b) type-2 CaO cube

Figure 10 presents the detachment of the solid $2CaO{\cdot}SiO_2$ from the region of interface between the CaO cube and slag. The sample shown in the Figure is Type-2, which is in the slag for 3 minutes at 1873 K. The stirring speed in this experiment is 100 rpm. As shown in the Figure, small pieces of $2CaO{\cdot}SiO_2$ phase have just detached from the interface region. The peninsulas of $2CaO{\cdot}SiO_2$ (marked as D) sticking out from the interface region are likely to be flushed off in the very next moment. This Figure shows evidently the main mechanism of the CaO dissolution when convection presents.

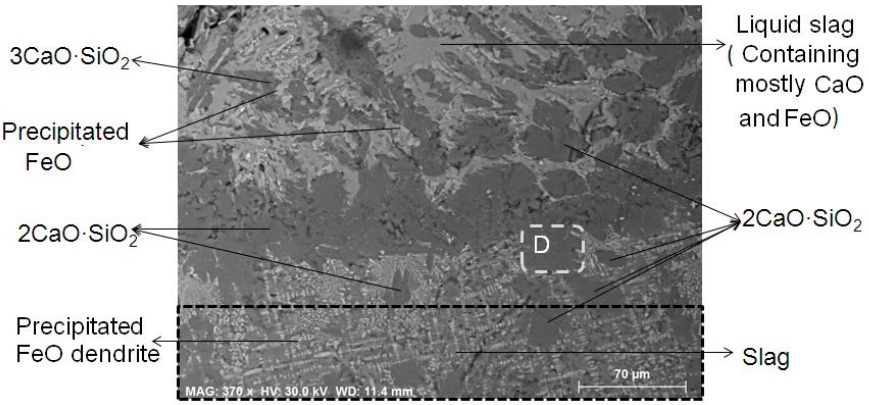

Figure 10 Detachment of the solid $2CaO{\cdot}SiO_2$ islands from the region of interface between the CaO cube and slag of Type-2 CaO cube after experiment at 100 rpm stirring speed for 3 minutes at 1873K

5. Discussion

As mentioned in the result part, the phases detected in all reacted samples are CaO, slag, $2CaO{\cdot}SiO_2$ and $3CaO{\cdot}SiO_2$. Solid FeO phase in dendrite form is also found in the slag. These phases are the same as in the previous work [26] for stagnant slag. A detailed discussion for the formation of these phases can be found in the previous publication.

On the other hand, the stirring would disturb the thermodynamic equilibrium, as the flow would transport the phases from one region to another. For example, $2CaO{\cdot}SiO_2$ islands are found in the slag as seen in figure 7. In spite of this stirring effect, an interface region is still clearly seen in all samples. This region consists of liquid phase, $2CaO{\cdot}SiO_2$

and $3CaO{\cdot}SiO_2$. A slag infiltrated zone is found just next to the interface. In this region, the SiO_2 content in infiltrating slag is very low, as it has been picked up by the CaO forming $3CaO{\cdot}SiO_2$. The small particles of $3CaO{\cdot}SiO_2$ are also found in the slag infiltrated region. The thermodynamic explanation for the formation of this region can be found in the previous work. [26]

It is reported in a previously study [26] that different limes samples do not show substantial difference in dissolution rate, when only natural convention and diffusion occur. The great difference in dissolution rate between the different types of lime (Figure 7) shows evidently that forced convection plays crucial role in lime dissolution in slag. Type-2 lime shows considerably slower dissolution rate in comparison with type-1 and type-3.

The previous study [26] reports that a dense layer of $2CaO.SiO_2$ is responsible for the total stop of the dissolution after the initial period. It suggests that constant removal of the $2CaO.SiO_2$ layer would be of essence to obtain high dissolution rate of lime. This suggestion is in line with the hypothesis of Natalie and Evans [11]. They pointed out that dicalcium silicate is swept into bulk slag by motion of the slag.

The peeling off of the $2CaO{\cdot}SiO_2$ layer by shear stress at the slag-lime interface is evidently seen in Figure 10. Small $2CaO{\cdot}SiO_2$ islands are found outside the interface region. A discontinue $2CaO{\cdot}SiO_2$ layer with zigzag shape is still visible in the interface region. The Figure even shows that some small peninsulas of $2CaO{\cdot}SiO_2$ are detaching from the layer. The Figure suggests strongly the removal of the dense $2CaO{\cdot}SiO_2$ layer is mainly due to the mechanical peeling off, but not due to chemical dissolution. Note that no $2CaO{\cdot}SiO_2$ islands are found far away from the slag-lime interface. It indicates that the islands peeled off by the shear stress from the layer dissolve into the slag on their way transported away from the cube.

The linear relationship between L_N and time in Figure 7 is also in accordance with above discussion. If the dissolution is controlled by chemical dissolution and mass transfer, the reaction rate should depend on the CaO concentration in the slag, which in turn depends on time. The linear relationships indicate the reaction rate is independent of time and therefore independent of CaO content. Hence, the dominating mechanism of the lime dissolution under the present condition is the mechanical removal of the $2CaO{\cdot}SiO_2$ product.

A comparison of the SEM microphotographs in Figure 8b and Figure 9b indicates that the increase of stirring speed has little effect on the morphology of the lime-slag interface region for Type-2 samples. On the other hand, the stirring speed has great effect on the morphology of Type-1 (see Figures 8a and 9a). In the case of dense lime like Type-2, the penetration of liquid slag into the CaO matrix is very limited. The shear stress due to the relative movement of the lime cube would only help, to some extent to remove the interface layer especially the $2CaO.SiO_2$ phase. This removal is the dominating mechanism for the lime dissolution. On the other hand, a lot liquid slag has infiltrated into the CaO matrix close to the interface in the Type-1 sample (see Figure 8a). The volume fraction of the liquid phase is almost about 0.5. At low stirring speed, e.g. 50 rpm as in the case of Figure 8a, the shear stress is not strong enough to remove the interface layer along with the slag infiltrated region. The increase of the stirring increases the relative velocity between the cube and the liquid slag. The slag infiltrated region close to the interface would be peeled off by the shear stress. The absence of the liquid infiltrated region in Figure 9a evidently supports this reasoning. A fast removal of the

$2CaO{\cdot}SiO_2$ layer would keep the lime surface "fresh" and make its dissolution continue without hindrance. The removal of the liquid infiltrated matrix along with the $2CaO.SiO_2$ layer would considerably enhance the lime dissolution. This would explain why Type-1 and Type-2 samples have a difference of L_N of 0.4 after 6 minutes. Note that the difference in L_N between these two types of limes is only 0.1 without stirring. [26]

6. Conclusion

The suitability of using rotating rod method to study the lime dissolution in slag was examined by CFD calculation and cold model experiments. No radial velocity would be generated by the concentrically placed long rotating rod. The minor forced convection, if any, introduced by the rotating rod made this method unsuitable for the study of lime dissolution under the condition of forced convection. This conclusion is in accordance with the criteria given in the pioneer work that the method should be used with big disk (big diameter/thickness ratio) in an infinity big bath.

To study the lime dissolution in slag under forced convection, a new experimental method was developed. A high temperature experimental setup was built up. Lime sample in the form of cube was employed. The detachment of $2CaO.SiO_2$ particles from the lime-slag interface was evidently seen. The main dissolution mechanism was found to be the removal of the interface layer(s) including the $2CaO.SiO_2$ phase by shear stress. This conclusion was drawn based on the microphotographs of the quenched samples consisting of both remaining lime and slag. The linear relationship between L_N and reaction time further supported this conclusion, as the dissolution was independent of the CaO concentration.

Acknowledgement

The authors are thankful to Professor Patrice Nortier and Dr Thierry Chopin for their valuable suggestions and stimulating discussions. Financial support from Lhoist is gratefully acknowledged.

Reference

[1] R. O. Russell: J. Metal, Vol. 19 (1967), pp. 104-106.
[2] W. J. Schlitt and G. W. Healey: Am. Ceram. Soc. Bull, Vol. 59 (1971), 954-957
[3] L. Hachtel, W. Fix and G. Trömel: Arch. Eisenhuttenw., Vol. 43 (1972), pp. 361-369
[4] H. Kimura, T. Yanagase, F. Noguchi and Y. Ueda: J. Jpn. Inst. Met., Vol. 38 (1974), pp. 226-232.
[5] T. Hamano, S. Fukagai and F. Tsukihashi: ISIJ International, Vol. 46 (2006), No. 4, pp. 490–495
[6] S. Amini, M. Brungs and O. Ostrovski: ISIJ International, Vol. 47 (2007), No. 1, pp. 32–37
[7] J. Yang, M. Kuwabara, T. Asano, A. Chuma, and J. Du: ISIJ International, Vol. 47 (2007), No. 10, pp. 1401–1408
[8] L. Elliott, S. M. Wang, T. Wall, F. Novak, J. Lucas, H. Hurst, J. Patterson, and J. Happ: Fuel Processing Technology, Vol. 56 (1998) pp. 45-53
[9] Y. Satyoko, W. E. Lee, E. Parry, P. Richards and I. G. Houldsworth: Ironmaking and Steelmaking, Vol. 30 (2003) No. 3, pp. 203-208
[10] M. Matsushima, S. Yadoomaru, K. Mori and Y. Kaxai: Tans. Iron Steel Inst. Jpn., Vol. 17 (1977), 442-449.
[11] C. A. Natalie, J. W. Evans: Ironmaking Steelmaking, 6 (1979), No. 3, 101-109
[12] R. P. Singh, D. N. Ghosh: Translations of the Indian Institute of Metals, Vol. 38 (1985) 207-214

[13] A. R. Cooper, W. D. Kingery: J. Am. Ceram. Soc. 47 (1964), No. 1, 37-43.
[14] M. Kosaka, S. Minowa: Tetsu-to-Hagane, 52 (1966), No. 12, 22-36
[15] A. Mitchell, B. Burel: Metall. Mater. Trans. B, Vol. 1 (1970), 2253-2256,
[16] T. Hamano, M. Horibe, K. Ito: ISIJ International, Vol. 44 (2004), No. 2, 263–267
[17] R. J. Fruehan, Y. Li, L. Brabie: Iron & Steel Society International Technology Conference and Exposition 2003; Indianapolis, IN; USA; 27-30 Apr. 2003, 799-812
[18] S.A. Nightingale, G.A. Brooks, B.J. Monahan: Metall. Mater. Trans. B, Vol. 36 (2005), No. 4, 453-461
[19] K. H. Sandhage, G. J. Yurek: J. Am. Ceram. Soc. Vol. 73(1990), No.12, 3633-3642
[20] M. Umakoshi, K. Mori, Y. Kawai: Transactions ISIJ, Vol. 24 (1984), 532-539
[21] A. H. Bui, H. M. Ha, Y. B. Kang, I. S. Chung, H. G. Lee: ISIJ International, Vol.45 (2005), No. 12, 1856-1863
[22] X. Yu, R.J. Pomfret, and K.S. Coley: Metall. Mater. Trans. B, Vol. 28 (1997), No. 2, 275-279
[23] J. Y. Choi, H. G. Lee, J. S. Kim: ISIJ International, Vol. 42 (2002), No.8, 852-860
[24] M. Lee, S. Sun, S. wright, S. Jahashahi: Metall. Mater. Trans. B 2001 Vol. 32B, 25-29
[25]D. P. Gregory and A. C. Riddiford: J. Chem. Soc., 1956, Vol. 3 3756-3764
[26] T. Deng, J. Gran, D. Sichen: Steel research int. Vol. 81 (2010), No. 5, 347-355